Journal of Applied Fluid Mechanics, Vol. 14, No. 3, pp. 805-817, 2021.
Available online at www.jafmonline.net, ISSN 1735-3572, EISSN 1735-3645.
DOI: 10.47176/jafm.14.03.31895

Numerical Simulation of Mass Transfer in Pulsatile Flow of Blood Characterized by Carreau Model under Stenotic Condition

Su. Mukhopadhyay[1], M. Shankar Mandal[2] and Sw. Mukhopadhyay[3]

[1]*Department of Mathematics, Acharya P. C. Roy Govt. College, Siliguri, W.B., India*
[2]*Department of Mathematics, G.G.D.C at Kalna-I, Purba Bardhaman-713405, W.B., India*
[3]*Department of Mathematics, The University of Burdwan, Burdwan-713104, W.B., India*

†*Corresponding Author Email: manimath@yahoo.com*

(Received June 3, 2020; accepted November 4, 2020)

ABSTRACT

The present numerical study deals with a mathematical model representing mass transfer in blood flow under stenotic condition. Streaming blood is considered as a non-Newtonian fluid characterized by Carreau fluid model and the vessel wall is taken to be flexible. The nonlinear pulsatile flow phenomenon is governed by the Navier-Stokes equations together with the continuity equation while that of mass transfer is governed by the convection-diffusion equation coupled with the velocity field. A finite difference scheme is developed to solve these equations accompanied bysuitable initial and boundary conditions. Results obtained are examined for numerical stability up to wanted degree of correctness. Various significant hemodynamic parameters are examined for additional qualitative insight of the flow-field and concentration-field over the entire arterial segment with the help of the obtained numerical results. Comparisons are made with the available results in open literature and good agreement has been achieved between these two results. Comparisons have been made to understand the effects of viscosity models for Newtonian and non-Newtonian fluids and also for rigid and flexible arteries.

Keywords: Non-Newtonian fluid; Carreau fluid model; Pulsatile flow; Mass transfer; Flexible artery.

1. INTRODUCTION

Partial occlusion of arteries, known as arterial stenosis, is one of the most frequent anomalies in cardiovascular system. Due to accumulation of low-density lipoprotein and other lipid bearing materials in streaming blood, such type of constrictions are formed (Ross 1993) and the disease thus caused by is called atherosclerosis. Under physiological conditions, atherosclerotic plaques may burst with no notice and as a result heart attack and stroke occur (Haque *et al*. 2014). Though the accurate grounds behind thecommencement of such constriction are not yet clearly known but it is well recognized that once such constriction is shaped, the hemodynamic environment in the area of the constriction is drastically changed and fluid dynamic factors take part in the propagation of the disease (Friedman *et al*. 1992; Smedby 1997; Liepsch 2002). Such obstruction in arteries implies that the transport of low-density lipoproteins from blood stream onto the arterial wall must play a key role in the development of stenotic lesions. Moreover, mechanical stresses are created by the interactions of plaque with the flow of blood leading to its burst. Recirculation region is formed downstream the plaque (Haque *et al*. 2014).

The flow disturbances associated with a medium degree of stenosis can be detected through the use of non-invasive methods such as the Doppler ultra-sound technique, but a method to detect a mild stenosis is still out of hand. The ability to describe the flow through constricted arteries may provide the possibility of diagnosing the disease in its earlier stages, even before the stenosis become clinically relevant, and is the basis for surgical intervention. Computational fluid dynamics provides a useful and non-invasive tool to study the hemodynamic factors, suspected to be associated with the propagation of atherosclerosis, through stenosed arteries (Pontrelli 2001).

During the past few decades, several studies on fluid dynamics through constricted arteries have been carried out to evaluate the flow pattern and the wall shear stress under steady and pulsatile flow

conditions (Tu *et al*. 1992, Misra and Chakravarty 1986, Mukhopadhyay *et al*. 2011 , Mandal *et al*. 2014, Mukhopadhyay *et al*. 2018a and Mukhopadhyay *et al*. 2019). Most of these numerical studies considered blood as a Newtonian fluid.

Experimental results reveal that blood behaves as a non-Newtonian fluid at low shear rates and in vessels of small cross-section (Ku 1997). Since the shear rate drops down significantly in the downstream side of a stenosis, Newtonian behavior of blood is not accurately applicable in the vicinity of a stenosis. Also, blood exhibits remarkably shear-thinning and visco-elastic behaviors in pulsatile flows (Phillips and Deutsch 1975). Several non-Newtonian models for viscosity of blood are available in literature. Unfortunately few research works have been carried out to study the hemodynamics in a stenosed artery by considering blood as a non-Newtonian fluid (Nakamura and Sawada 1990; Misra *et al*. 1993; Pontrelli 2001; Mandal *et al*. 2012; Nandakumar *et al*. 2015 and Mukhopadhyay *et al*. 2018a). With the help of Carreau model, Ali *et al*. (2015) analyzed the unsteady blood flow through a tapered catheterized vessel having an overlapping stenosis. Using Casson model and generalized Maxwell model, Nejad *et al*. (2018) investigated the pulsatile flow of blood in a viscoelastic artery having a symmetric constriction. It is more surprising that regardless of significance of non-Newtonian fluid, Carreau viscosity model has been received less attention compared to other non-Newtonian fluid models. Of late, considering Carreau model, Attia *et al*. (2018) investigated the blood flow under stenotic condition for diabetic and normal persons.

Although formation and development of atherosclerotic lesions are often found positively correlated with low and oscillatory wall shear stress (Ku *et al*. 1985), some researchers believe that wall shear stress may not be the only responsible mechanism for such intimal thickening. Caro *et al*. (1971) suggested that stenosis may also occur due to mass transfer mechanism of fatty substances from blood onto arterial wall. Furthermore, a clear understanding of mass transport in arterial stenoses is of significant medical interest in the inspection of the creation and progress of atherosclerotic lesions. Thus to identify the possible sites of atherogenic depositions, it is crucial to study the behaviour of local mass transport. Basically, mass transfer refers to the movement of blood-borne components such as oxygen and LDLs (Low-Density Lipoproteins) from streaming blood into the arterial walls or vice versa.A number of studies about the local mass transport phenomenon in a constricted tube may be found in literature (Ma *et al*. 1994; Rappitsch *et al*. 1997; Kaazempur-Mofrad *et al*. 2005; Sarifuddin *et al*. 2009 and Zaman *et al*. 2016). Recently, Zaman *et al*. (2016) reported the combined effects of unsteadiness and tapering on heat and mass transfer in blood flow obeying Cross viscosity model under stenotic condition. Tripathi and Sharma (2020) analyzed the effects of Joule heating, magnetic field and variable viscosity on heat and mass transfer of two phase blood flow.

Unfortunately, most of the existing studies in this field are either incomplete or are not representative of the actual arterial flow. Non-Newtonian behaviour of blood, flexibility of arterial wall, physiologically realistic pulsatile flow of blood all are not taken into account in any of the aforementioned studies. Therefore, in this numerical study, a sincere attempt has been taken to include all of these characteristics of actual arterial flow. It is assumed that the arterial segment is a cylindrical tube with time-variant wall geometry and streaming blood is non-Newtonian characterized by the Carreau viscosity model. The unsteady nonlinear Navier-Stokes equations in cylindrical coordinates governing blood flow and the mass transport equation coupled to the velocity field are taken up along with appropriate boundary conditions and are solved using the stream function-vorticity approach. To validate the applicability of the present model, large-scale numerical computations have been carried out and appropriate scientific discussions were made to understand the effects of various hemodynamic parameters on wall shear stress, local mass transfer rate etc. In addition, the quantitative analysis is carried out which includes the flow structure and distribution of concentration.

2. BLOOD VISCOSITY MODEL

Though the Newtonian approximation for blood viscosity is acceptable in large arteries, a non-Newtonian constitutive equation should be used to describe blood flow in smaller arteries. The plasma may be regarded as a Newtonian fluid, but when one considers its contents, especially red blood cells, the viscosity of the mixture increases significantly. Experimental results show that the viscosity of blood decreases as shear rate increases. In literature, different constitutive equations have been proposed to model the shear thinning viscosity of blood.

Due to broader span of shear rates, Carreau fluid model is best fitted for blood flow through arteries of both larger and smaller diameters (Razavi *et al*. 2011; Ali *et al*. 2015; Attia *et al*. 2018). The shear dependent Carreau viscosity model is a four parameter shear thinning model and is described as:

$$\mu^*(\dot{\gamma}^*) = \mu_\infty + (\mu_0 - \mu_\infty)\left(1 + \Lambda^{*2}\dot{\gamma}^*\right)^{(n-1)/2} \quad (1)$$

where $\dot{\gamma}^*$ is the shear rate, μ_0 and μ_∞ are the asymptotic apparent viscosities of blood as $\dot{\gamma}^* \to 0$ and ∞ respectively, $\Lambda^* \geq 0$ is a material constant with the dimension of time representing the degree of shear thinning. Values of these parameters for human blood, found in literature, are $\mu_0 = 0.056$ Pa s, $\mu_\infty = 0.00345$ Pa s, $\Lambda^* = 3.313$ s, $n = 0.3568$ (Cho and Kensey 1991). When $\mu^*(\dot{\gamma}^*) = \mu_\infty$, Newtonian model is obtained.

3. FORMULATION OF THE PROBLEM

3.1. Governing Equations

Let us consider the pulsatile laminar incompressible

and axi-symmetric flow of blood with constant density ρ and shear dependent viscosity $\mu^*(r^*)$ flowing through an axi-symmetric artery with a bell-shaped axi-symmetric constriction. The axis of the arteryis taken as the z-axis of a cylindrical polar coordinate system(r^*, θ^*, z^*). Since we are looking for an axi-symmetric two-dimensional solution, all variables may be assumed to be independent of θ^*(Pontrelli 2001). Let $R_0(t^*)$be the radius of the arteryat the inlet and $r_0^*(z^*, t^*)$ defines the wall of the arteryat time t^*. The origin O is taken at the inlet. Also, let p^* be the pressure, u^* and v^* be the velocity components along the axial and radial directions respectively and C^* be the concentration field of the solute. For pulsatile flow, the flow rate is time dependent. Let us introduce the following dimensionless quantities

$$z = \frac{z^*}{R_0}, r = \frac{r^*}{R_0}, r_0 = \frac{r_0^*}{R_0}, u = \frac{u^*}{U_0}, v = \frac{v^*}{U_0},$$
$$t = \frac{t^*}{T}, p = \frac{p^*}{\rho U_0^2}, C = \frac{C^*}{C_s},$$
$$\lambda = \frac{\mu_0}{\mu_\infty}, \Lambda = \frac{\Lambda^* U_0}{R_0}, \mu = \frac{\mu^*}{\mu_\infty}, \quad (2)$$

where, U_0 is the centerline velocity at the inlet,T is the periodic timeof the pulsatile flow and C_s is the reference concentration at the inlet.

The unsteady, two dimensional Navier-Stokes equations of a homogeneous incompressible fluid may be written in dimensionless form as

$$\mathrm{St}\frac{\partial u}{\partial t} + \frac{\partial (uv)}{\partial r} + \frac{\partial (u^2)}{\partial z} + \frac{uv}{r} = -\frac{\partial p}{\partial z} + \frac{1}{\mathrm{Re}}\left[\mu\left(\frac{\partial^2 u}{\partial r^2} + \frac{1}{r}\frac{\partial u}{\partial r} + \frac{\partial^2 u}{\partial z^2}\right) + \frac{\partial \mu}{\partial r}\left(\frac{\partial u}{\partial r} + \frac{\partial v}{\partial z}\right) + 2\frac{\partial \mu}{\partial z}\frac{\partial u}{\partial z}\right] \quad (3)$$

and

$$\mathrm{St}\frac{\partial v}{\partial t} + \frac{\partial (v^2)}{\partial r} + \frac{\partial (uv)}{\partial z} + \frac{v^2}{r} = -\frac{\partial p}{\partial r} + \frac{1}{\mathrm{Re}}\left[\mu\left(\frac{\partial^2 v}{\partial r^2} + \frac{1}{r}\frac{\partial v}{\partial r} + \frac{\partial^2 v}{\partial z^2} - \frac{v}{r^2}\right) + 2\frac{\partial \mu}{\partial r}\frac{\partial v}{\partial r} + \frac{\partial \mu}{\partial z}\left(\frac{\partial v}{\partial z} + \frac{\partial u}{\partial r}\right)\right]. \quad (4)$$

Also the equation of continuity is

$$r\frac{\partial u}{\partial z} + \frac{\partial (vr)}{\partial r} = 0. \quad (5)$$

Here, $\mathrm{Re} = U_0 R_0 \rho/\mu_\infty$ is the flow Reynolds number and $\mathrm{St} = R_0/(U_0 T)$ is the Strouhal number.

The convection-diffusion equation governing the flow of mass transport in the blood stream may be written in terms of non-dimensional variables as

$$\mathrm{St}\frac{\partial \mathrm{C}}{\partial \mathrm{t}} + u\frac{\partial \mathrm{C}}{\partial z} + v\frac{\partial \mathrm{C}}{\partial r} = \frac{1}{\mathrm{ReSc}}\left[\frac{\partial^2 \mathrm{C}}{\partial r^2} + \frac{1}{r}\frac{\partial \mathrm{C}}{\partial r} + \frac{\partial^2 \mathrm{C}}{\partial z^2}\right]. \quad (6)$$

Here, $\mathrm{Sc} = \frac{\mu}{\rho D}$ is theSchmidt number, D being the coefficient of diffusion.

The dimensionless blood viscosity is obtained as

$$\mu(\dot{\gamma}) = 1 + (\lambda - 1)\{1 + \Lambda^2\dot{\gamma}\}^{(n-1)/2} \quad (7)$$

with

$$\dot{\gamma} = \left[2\left(\frac{\partial u}{\partial z}\right)^2 + 2\left(\frac{\partial v}{\partial r}\right)^2 + 2\left(\frac{v}{r}\right)^2 + \left(\frac{\partial u}{\partial r} + \frac{\partial v}{\partial z}\right)^2\right]^{1/2}. \quad (8)$$

$\lambda = 1$ refers to the Newtonian model.

3.2. Geometry of the Tube

The geometry of the arterial segment with a smooth axi-symmetric constriction in it may be described in dimensionless form as:

$$r_0(z,t) = \left[1 - \delta e^{-\sigma(z-a)^2}\right]a_1(t), 0 \le z \le L \quad (9)$$

where a and δ indicate the centre and height of the stenosis, σ represents the rate at which the boundary profile changes and L is the length of the arterial segment under consideration. In our study we have taken $\sigma = 5, a = 4, L = 10$.

As the wall movement must be proportional to the flow rate, the time-variant parameter $a_1(t)$ is chosen as

$$a_1(t) = 1 + k|Q(t) - Q(0)| \quad (10)$$

where k is the amplitude parameterand $Q(t)$ is the pulsatile flow rate. As formation of stenosis significantly reduces the distiensibility of vessel wall (Davies *et al*. 1985; Nerem 1992), a small value $k = 0.01$ is used in this study.

Schematic diagrams of the flexible artery have been presented in Fig.1(A)-(B).Figure 1(A) exhibits the geometry of flexible artery for various constriction heights δ at t=0.13 whereas the effects of flexibility can be found in Fig.1(B) which portraits the geometry of the artery at two different times.

4. STREAMFUNCTION-VORTICITY FORMULATION

Let us now define the dimensionless Stokes stream function $\psi(z, r, t)$ by

$$u = \frac{1}{r}\frac{\partial \psi}{\partial r}, v = -\frac{1}{r}\frac{\partial \psi}{\partial z}, \quad (11)$$

and the corresponding azimuthal vorticity function $\omega(z, r, t)$ by

$$\omega = \frac{\partial v}{\partial z} - \frac{\partial u}{\partial r}. \quad (12)$$

Cross-differentiation of the momentum Eq. (3) and Eq. (4), with use of Eq. (11) and Eq. (12), yields

$$St\frac{\partial \omega}{\partial t} + u\frac{\partial \omega}{\partial z} + v\frac{\partial \omega}{\partial r} - \frac{v\omega}{r} = \frac{1}{Re}\left[\mu\left(\frac{\partial^2 \omega}{\partial z^2} + \frac{\partial^2 \omega}{\partial r^2} + \frac{1}{r}\frac{\partial \omega}{\partial r} - \frac{\omega}{r^2}\right) + 2\frac{\partial \mu}{\partial z}\frac{\partial \omega}{\partial z} + \frac{\partial \mu}{\partial r}\left(2\frac{\partial \omega}{\partial r} + \frac{\omega}{r}\right) - 2\frac{\partial^2 \mu}{\partial r \partial z}\left(\frac{v}{r} + 2\frac{\partial u}{\partial z}\right) + \left(\frac{\partial^2 \mu}{\partial z^2} - \frac{\partial^2 \mu}{\partial r^2}\right)\left(\frac{\partial u}{\partial r} + \frac{\partial v}{\partial z}\right)\right] \quad (13)$$

Also, the equation of continuity, with the use of Eq. (11) and Eq. (12), transforms to the Poisson equation given by

$$\frac{\partial^2 \psi}{\partial z^2} + \frac{\partial^2 \psi}{\partial r^2} - \frac{1}{r}\frac{\partial \psi}{\partial r} = -\omega r \quad (14)$$

5. INITIAL AND BOUNDARY CONDITIONS

The initial conditions for the velocity and concentration field are set as

$$u = \frac{2Q(0)}{\pi r_0^2}\left\{1 - \left(\frac{r}{r_0}\right)^2\right\}, v = 0, C = 1 - \left(\frac{r}{r_0}\right)^2. \quad (15)$$

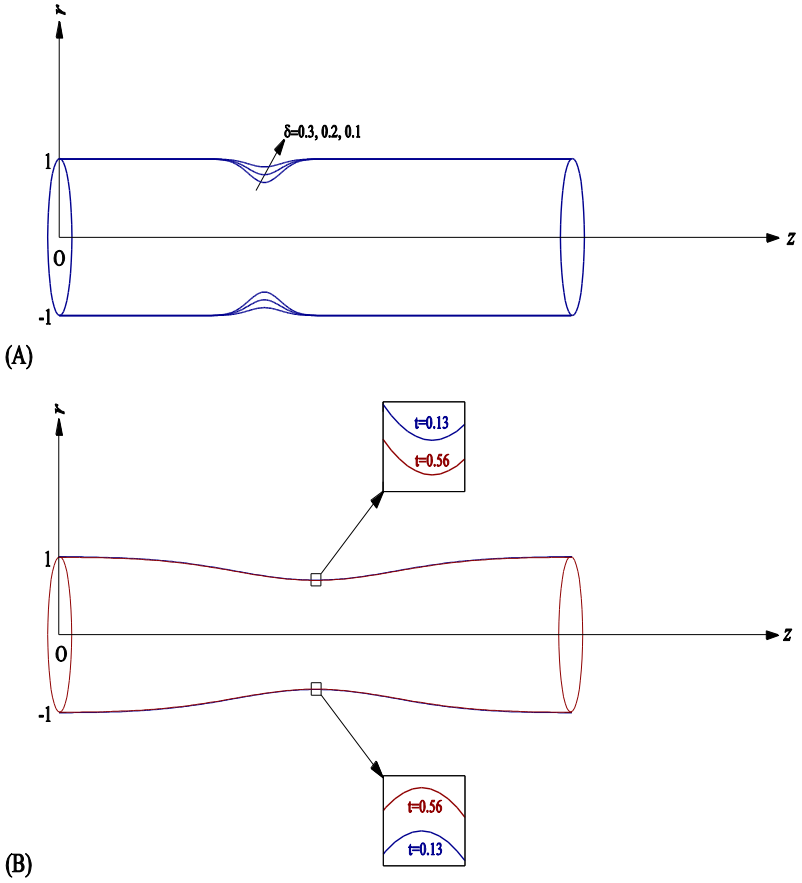

Fig. 1. Geometry of the flexible tube (A) for different constriction heights at $t = 0.14$ (B) for different times.

Though the initially chosen velocity or concentration fields are not physiological, it is found that final results do not depend on these profiles. Further it is found that the results do not change significantly when the simulation runs for more than three time periods. Therefore, the simulation is carried out up to three time periods in all cases so that all transitional effects vanish within these three time periods.

For the boundary conditions at the inlet cross section of the tube, the flow is assumed to be fully developed i.e.

$$\frac{\partial \omega}{\partial z} = \frac{\partial \psi}{\partial z} = 0 \text{ at } z = 0 \tag{16}$$

and at the outlet cross section, the flow field is assumed to have no change which gives

$$\frac{\partial^2 \omega}{\partial z^2} = \frac{\partial^2 \psi}{\partial z^2} = 0 \text{ at } z = L. \tag{17}$$

The flow symmetry gives the conditions

$$\psi = 0, \omega = 0 \text{ along } r = 0. \tag{18}$$

The usual 'no slip' condition is imposed on the tube wall which gives

$$\frac{\partial \psi}{\partial r} = 0 \text{ along } r = r_0(z,t). \tag{19}$$

Due to the movement of the vessel wall, radial velocity at the wall is equal to $\frac{\partial r_0}{\partial t}$ and hence

$$\frac{\partial \psi}{\partial z} = -r_0 \frac{\partial r_0}{\partial t} \text{ along } r = r_0(z,t). \tag{20}$$

The axial symmetry condition for the concentration field gives

$$\frac{\partial C}{\partial r} = 0 \text{ along } r = 0. \tag{21}$$

At the inlet, the concentration of the solute is assumed to be constant while the concentration gradient at the outlet is assumed to be zero. Thus

$$C = 1 \text{ at } z = 0 \text{ and } \frac{\partial C}{\partial z} = 0 \text{ at } z = L. \tag{22}$$

A Dirichlet boundary condition of the zero concentration on the arterial wall (Etheir 2002; Sarifuddin *et al.* 2009; Zaman *et al.* 2016) is set as

$$C = 0 \text{ at } r = r_0(z,t). \tag{23}$$

A time dependent non-dimensional pulsatile flow rate

$$Q(t) = Q^*(t)/Q^*_{\max}(t) \tag{24}$$

is given through the tube (see Fig.2(A), where $Q^*(t)$ is a physiologically realistic pulsatile flow rate of blood as

given by Stettler *et al.* (1981). Since the mass flux across all cross-sections of the tube is the same at any instant of time, so

$$\int_0^{r_0(z,t)} 2\pi r\left(\frac{1}{r}\frac{\partial\psi}{\partial r}\right)dr = Q(t).$$

This gives the value of the stream function ψ at the tube wall as

$$\psi(z, r_0(z,t), t) = \frac{1}{2\pi}Q(t). \tag{25}$$

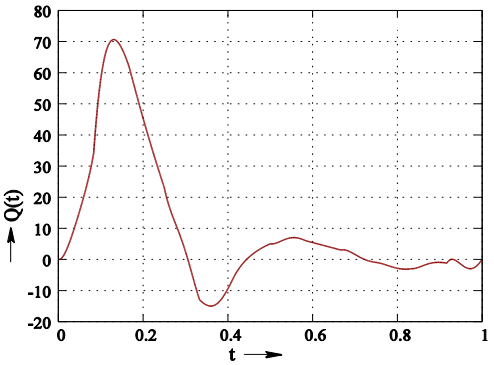

Fig. 2(A). Physiological pulsatile flow rate of Stettler *et al.* (1981).

6. COORDINATE TRANSFORMATION

Let us choose a suitable coordinate system so that the arterial constriction coincides with a constant coordinate curve. For this, let us introduce a radial coordinate transformation given by Ling and Atabek (1972),

$$x = \frac{r}{r_0(z,t)}, \tag{26}$$

which maps the constricted region into a rectangular one. Using this transformation, the vorticity transport Eq. (12) is transformed into

$$\mathrm{St}\left(\frac{\partial\omega}{\partial t} - \frac{x}{r_0}\frac{\partial r_0}{\partial t}\frac{\partial\omega}{\partial x}\right) + u\left(\frac{\partial\omega}{\partial z} - \frac{x}{r_0}\frac{\partial r_0}{\partial z}\frac{\partial\omega}{\partial x}\right) + \frac{v}{r_0}\frac{\partial\omega}{\partial x} - \frac{v\omega}{xr_0}$$

$$= \frac{1}{\mathrm{Re}}\left[\mu\left\{\frac{\partial^2\omega}{\partial z^2} + \left(\frac{x^2}{r_0^2}\left(\frac{\partial r_0}{\partial z}\right)^2 + \frac{1}{r_0^2}\right)\frac{\partial^2\omega}{\partial x^2} - \frac{2x}{r_0}\frac{\partial r_0}{\partial z}\frac{\partial^2\omega}{\partial x\partial z} + \left(\frac{2x}{r_0^2}\left(\frac{\partial r_0}{\partial z}\right)^2 - \frac{x}{r_0}\frac{\partial^2 r_0}{\partial z^2} + \frac{1}{xr_0^2}\right)\frac{\partial\omega}{\partial x} - \frac{\omega}{x^2 r_0^2}\right\}\right.$$

$$+2\left(\frac{\partial\mu}{\partial z} - \frac{x}{r_0}\frac{\partial r_0}{\partial z}\frac{\partial\mu}{\partial x}\right)\left(\frac{\partial\omega}{\partial z} - \frac{x}{r_0}\frac{\partial r_0}{\partial z}\frac{\partial\omega}{\partial x}\right) + \frac{1}{r_0}\frac{\partial\mu}{\partial x}\left(\frac{2}{r_0}\frac{\partial\omega}{\partial x} + \frac{\omega}{xr_0}\right) - \frac{2}{r_0}\left(\frac{\partial^2\mu}{\partial x\partial z} - \frac{1}{r_0}\frac{\partial r_0}{\partial z}\frac{\partial\mu}{\partial x} - \frac{x}{r_0}\frac{\partial r_0}{\partial z}\frac{\partial^2\mu}{\partial x^2}\right)\left(\frac{v}{xr_0} + 2\frac{\partial u}{\partial z} - \frac{2x}{r_0}\frac{\partial r_0}{\partial z}\frac{\partial u}{\partial x}\right) + \left\{\frac{\partial^2\mu}{\partial z^2} + \left(\frac{x^2}{r_0^2}\left(\frac{\partial r_0}{\partial z}\right)^2 - \frac{1}{r_0^2}\right)\frac{\partial^2\mu}{\partial x^2} - \frac{2x}{r_0}\frac{\partial r_0}{\partial z}\frac{\partial^2\mu}{\partial x\partial z} + \left(\frac{2x}{r_0^2}\left(\frac{\partial r_0}{\partial z}\right)^2 - \frac{x}{r_0}\frac{\partial^2 r_0}{\partial z^2}\right)\frac{\partial\mu}{\partial x}\right\}\left(\frac{1}{r_0}\frac{\partial u}{\partial x} + \frac{\partial v}{\partial z} - \frac{x}{r_0}\frac{\partial r_0}{\partial z}\frac{\partial v}{\partial x}\right)\right]. \tag{27}$$

Vorticity and stream function are related by the following equation

$$\frac{\partial^2\psi}{\partial z^2} + \left\{\frac{x^2}{r_0^2}\left(\frac{\partial r_0}{\partial z}\right)^2 + \frac{1}{r_0^2}\right\}\frac{\partial^2\psi}{\partial x^2} - \frac{2x}{r_0}\frac{\partial r_0}{\partial z}\frac{\partial^2\psi}{\partial x\partial z} + \left\{\frac{2x}{r_0^2}\left(\frac{\partial r_0}{\partial z}\right)^2 - \frac{x}{r_0}\frac{\partial^2 r_0}{\partial z^2} - \frac{1}{xr_0^2}\right\}\frac{\partial\psi}{\partial x} = -r_0 x\omega. \tag{28}$$

The transformed boundary condition for the stream function ψ at $x = 1$ becomes

$$\psi(z, x = 1, t) = \frac{1}{2\pi}Q(t). \tag{29}$$

To derive a boundary condition for the vorticity ω at $x = 1$, we use Eq. (28) and obtain

$$\omega(z, x = 1, t) = -\frac{1}{r_0^3}\left[1 + \left(\frac{\partial r_0}{\partial z}\right)^2\right]\left(\frac{\partial^2\psi}{\partial x^2}\right)_{x=1} + \left(\frac{\partial^2 r_0}{\partial z\partial t} + \frac{1}{r_0}\frac{\partial r_0}{\partial z}\frac{\partial r_0}{\partial t}\right). \tag{30}$$

The transformed form of the mass transport Eq. (6) is given by

$$\mathrm{St}\left(\frac{\partial C}{\partial t} - \frac{x}{r_0}\frac{\partial r_0}{\partial t}\frac{\partial C}{\partial x}\right) + u\left(\frac{\partial C}{\partial z} - \frac{x}{r_0}\frac{\partial r_0}{\partial z}\frac{\partial C}{\partial x}\right) + \frac{v}{r_0}\frac{\partial C}{\partial x} = \frac{1}{\mathrm{ReSc}}\left[\frac{1}{r_0^2}\frac{\partial^2 C}{\partial x^2} + \frac{1}{xr_0^2}\frac{\partial C}{\partial x} + \left\{\frac{\partial^2 C}{\partial z^2} + \frac{x^2}{r_0^2}\left(\frac{\partial r_0}{\partial z}\right)^2\frac{\partial^2 C}{\partial x^2} - \frac{2x}{r_0}\frac{\partial r_0}{\partial z}\frac{\partial^2 C}{\partial x\partial z} + \left(\frac{2x}{r_0^2}\left(\frac{\partial r_0}{\partial z}\right)^2 - \frac{x}{r_0}\frac{\partial^2 r_0}{\partial z^2}\right)\frac{\partial C}{\partial x}\right\}\right]. \tag{31}$$

7. NUMERICAL METHOD

The transformed governing equations together with the initial and boundary conditions are solved numerically by using finite difference technique over a uniformly spaced grid. The vorticity transport Eq. (27) and the equation for stream function Eq. (28) are discretized using central difference approximations for all spatial derivatives and forward difference approximation for the time derivative of ω.

The finite difference representations of the derivatives and all other terms have been written at the mesh point (i, j) which indicates a point where $z_i = i\Delta z$ and $x_j = j\Delta x$, Δz and Δx being the increments of z and x respectively. The finite difference form for time is written as $t_k = k\Delta t$, where Δt is the time increment.

A tri-diagonal system of algebraic equations associated with each line (constant i) in x-direction is formed. The finite-difference representation of Eq. (28) is

$$A(j)\psi_{i,j-1}^{k+1} + B(j)\psi_{i,j}^{k+1} + C(j)\psi_{i,j+1}^{k+1} = D(j) \tag{32}$$

where the quantities $A(j), B(j), C(j)$ and $D(j)$ are defined by

$$A(j) = \frac{L_2}{(\Delta x)^2} - \frac{L_1}{2\Delta x}, B(j) = -\frac{2}{(\Delta z)^2} - \frac{2L_2}{(\Delta x)^2}, C(j) = \frac{L_2}{(\Delta x)^2} + \frac{L_1}{2\Delta x}$$ and

$$D(j) = -r_0 x\omega_{i,j}^k - \frac{\psi_{i+1,j}^k + \psi_{i-1,j}^k}{(\Delta z)^2} + L_3\frac{\psi_{i+1,j+1}^k - \psi_{i+1,j-1}^k - \psi_{i-1,j+1}^k + \psi_{i-1,j-1}^k}{4\Delta z\Delta x}$$

in which

$$L_1 = \frac{2x}{r_0^2}\left(\frac{\partial r_0}{\partial z}\right)^2 - \frac{x}{r_0}\frac{\partial^2 r_0}{\partial z^2} - \frac{1}{xr_0^2}, L_2 = \frac{x^2}{r_0^2}\left(\frac{\partial r_0}{\partial z}\right)^2 + \frac{1}{r_0^2}, L_3 = \frac{2x}{r_0}\frac{\partial r_0}{\partial z}.$$

Using the values of all the quantities in $A(j), B(j), C(j)$ and $D(j)$ at the k^{th}-time level, the tri-diagonal system of Eq. (32) can be solved by using the well-known Thomas algorithm for each fixed i in x-direction, to get the value of the stream

function at the $(k+1)^{\text{th}}$-time level. Eq. (11) then gives the values of $u$and v.

We now use a second order accurate formula for wall vorticity obtained from Eq. (30) in terms of the known values of stream function. The vorticity at the tube wall is given by

$$\omega(z,x=1,t)=-\frac{2}{{r_0}^3}\left[1+\left(\frac{\partial r_0}{\partial z}\right)^2\right]\frac{\psi_{i,jstp-1}-\psi_{i,jstp}}{(\Delta x)^2}+\left(\frac{\partial^2 r_0}{\partial z\partial t}+\frac{1}{r_0}\frac{\partial r_0}{\partial z}\frac{\partial r_0}{\partial t}\right) \quad (33)$$

where $j=jstp$ corresponds to the value of x at the tube wall.

The momentum Eq. (27) is now solved exactly in the same way as stated above. The discretized form of the momentum Eq. (27) is given by

$$P(j)\omega_{i,j-1}^{k+1}+Q(j)\omega_{i,j}^{k+1}+R(j)\omega_{i,j+1}^{k+1}=S(j) \quad (34)$$

where the quantities $P(j),Q(j),R(j)$ and $S(j)$ are defined as

$$P(j)=\frac{1}{2\Delta x}\left(\frac{ux}{r_0}\frac{\partial r_0}{\partial z}-\frac{v}{r_0}\right)+\frac{1}{\mathrm{Re}}\left(\frac{M_1}{2\Delta x}-\frac{M_2}{(\Delta x)^2}\right)-M_3+M_4+\frac{\mathrm{St}}{2\Delta x}\frac{x}{r_0}\frac{\partial r_0}{\partial t},$$

$$Q(j)=\frac{\mathrm{St}}{\Delta t}-\frac{v}{xr_0}+\frac{2M_2}{\mathrm{Re}(\Delta x)^2}+\frac{\mu}{\mathrm{Re}(xr_0)^2}-\frac{1}{\mathrm{Re}\,{r_0}^2 x}\frac{\partial\mu}{\partial x},$$

$$R(j)=-\frac{1}{2\Delta x}\left(\frac{ux}{r_0}\frac{\partial r_0}{\partial z}-\frac{v}{r_0}\right)-\frac{1}{\mathrm{Re}}\left(\frac{M_1}{2\Delta x}+\frac{M_2}{(\Delta x)^2}\right)+M_3-M_4-\frac{\mathrm{St}}{2\Delta x}\frac{x}{r_0}\frac{\partial r_0}{\partial t}\text{ and}$$

$$S(j)=\frac{St}{\Delta t}\omega_{i,j}^k-u\frac{\omega_{i+1,j}^k-\omega_{i-1,j}^k}{2\Delta z}+\frac{\mu}{Re}\left(\frac{\omega_{i+1,j}^k-2\omega_{i,j}^k+\omega_{i-1,j}^k}{(\Delta z)^2}-\frac{x}{r_0}\frac{\partial r_0}{\partial z}\frac{\omega_{i+1,j+1}^k-\omega_{i+1,j-1}^k-\omega_{i-1,j+1}^k+\omega_{i-1,j-1}^k}{2\Delta z\Delta x}\right)+\frac{2}{\mathrm{Re}}\left(\frac{\partial\omega}{\partial z}-\frac{x}{r_0}\frac{\partial r_0}{\partial z}\frac{\partial\omega}{\partial x}\right)\frac{\omega_{i+1,j}^k-\omega_{i-1,j}^k}{2\Delta z}+\frac{M}{\mathrm{Re}}$$

in which $M_1=\mu\left[\frac{2x}{r_0^2}\left(\frac{\partial r_0}{\partial z}\right)^2-\frac{x}{r_0}\frac{\partial^2 r_0}{\partial z^2}+\frac{1}{xr_0^2}\right]$,

$$M_2=\mu\left[\frac{x^2}{r_0^2}\left(\frac{\partial r_0}{\partial z}\right)^2+\frac{1}{r_0^2}\right],$$

$$M_3=\frac{x}{\mathrm{Re}r_0\Delta x}\frac{\partial r_0}{\partial z}\frac{\partial\mu}{\partial z}\quad,\quad M_4=\frac{1}{\mathrm{Re}{r_0}^2\Delta x}\left[x^2\left(\frac{\partial r_0}{\partial z}\right)^2+1\right]\frac{\partial\mu}{\partial x},$$

$$M=-\frac{2}{r_0}\left(\frac{\partial^2\mu}{\partial x\partial z}-\frac{1}{r_0}\frac{\partial r_0}{\partial z}\frac{\partial\mu}{\partial x}-\frac{x}{r_0}\frac{\partial r_0}{\partial z}\frac{\partial^2\mu}{\partial x^2}\right)\left(\frac{v}{xr_0}+2\frac{\partial u}{\partial z}-\frac{2x}{r_0}\frac{\partial r_0}{\partial z}\frac{\partial u}{\partial x}\right)+\left\{\frac{\partial^2\mu}{\partial z^2}+\left(\frac{x^2}{r_0^2}\left(\frac{\partial r_0}{\partial z}\right)^2-\frac{1}{r_0^2}\right)\frac{\partial^2\mu}{\partial x^2}-\frac{2x}{r_0}\frac{\partial r_0}{\partial z}\frac{\partial^2\mu}{\partial x\partial z}+\left(\frac{2x}{r_0^2}\left(\frac{\partial r_0}{\partial z}\right)^2-\frac{x}{r_0}\frac{\partial^2 r_0}{\partial z^2}\right)\frac{\partial\mu}{\partial x}\right\}\left(\frac{1}{r_0}\frac{\partial u}{\partial x}+\frac{\partial v}{\partial z}-\frac{x}{r_0}\frac{\partial r_0}{\partial z}\frac{\partial v}{\partial x}\right)$$

The mass transport Eq. (31) is solved by using its discretized version

$$C_{i,j}^{k+1}=C_{i,j}^k+\frac{\Delta t}{\mathrm{St}}\left[N_4\frac{C_{i,j+1}^k-C_{i,j-1}^k}{2\Delta x}-u\frac{C_{i+1,j}^k-C_{i-1,j}^k}{2\Delta z}+\frac{1}{\mathrm{ReSc}}\left\{\frac{C_{i+1,j}^k-2C_{i,j}^k+C_{i-1,j}^k}{(\Delta z)^2}-N_3\frac{C_{i+1,j+1}^k-C_{i+1,j-1}^k-C_{i-1,j+1}^k+C_{i-1,j-1}^k}{4\Delta z\Delta x}+N_2\frac{C_{i,j+1}^k-2C_{i,j}^k+C_{i,j-1}^k}{(\Delta x)^2}+N_1\frac{C_{i,j+1}^k-C_{i,j-1}^k}{2\Delta x}\right\}\right]$$

where $N_1=\frac{2x}{r_0^2}\left(\frac{\partial r_0}{\partial z}\right)^2-\frac{x}{r_0}\frac{\partial^2 r_0}{\partial z^2}+\frac{1}{xr_0^2}, N_2=\frac{x^2}{r_0^2}\left(\frac{\partial r_0}{\partial z}\right)^2+\frac{1}{r_0^2},$

$N_3=\frac{2x}{r_0}\frac{\partial r_0}{\partial z}, N_4=\mathrm{St}\frac{x}{r_0}\frac{\partial r_0}{\partial t}+\frac{ux}{r_0}\frac{\partial r_0}{\partial z}-\frac{v}{r_0}.$

Once the velocity and concentration field of the streaming blood is obtained, the dimensionless wall shear stress and Sherwood number (Zierenberg *et al.* 2006), representing the local mass flux to the arterial wall, are computed by using the formulae

$$\tau_{\mathrm{w}}=-\left(\mu\frac{\partial u}{\partial r}\right)_{\mathrm{wall}} \quad (35)$$

and

$$Sh=-2\left(\frac{\partial C}{\partial r}\right)_{\mathrm{wall}} \quad (36)$$

The wall pressure is obtained by solving the coupled Eq. (3) and Eq.(4). For this a zero pressure at the inlet is assigned.

8. STABILITY CRITERIA OF THE NUMERICAL SCHEME

Some restrictions are imposed on selecting the time step Δt depending on the grid size$\Delta z,\Delta x$. The first restriction i.e. CFL (Courant *et al.* 1928) condition is given by

$$\Delta t_1\le \mathrm{Min}\left[\frac{\Delta z}{|u|},\frac{\Delta x}{|v|}\right]_{(i,j)}.$$

The second restriction is related to the viscous effect and is given by

$$\Delta t_2\le \mathrm{Min}\left[\frac{\mathrm{Re}}{2}\frac{\Delta z^2\Delta x^2}{\Delta z^2+\Delta x^2}\right]_{(i,j)}.$$

Actually, the time step is chosen by using the relation$\Delta t=\beta\mathrm{Min}[\Delta t_1,\Delta t_2], 0<\beta\le 1$, where the minimum is taken in the global sense and the time steps Δt_1 and Δt_2 must satisfy the above two inequalities. Inthe present study, the parameter β is selected as 0.1.

9. RESULTS AND DISCUSSION

In this study, a non-dimensional physiological pulsatile flow rate [see, Fig.2(A)] proposed by Stettler *et al.* (1981) has been considered. This flow profile includes flow reversal and is composed of, in each cycle, an impulsive motion with strong acceleration and deceleration (systole) followed by a slowly accelerating and decelerating flow (diastole). It may be characterized by the peak flow in systole ($t=0.14$), maximum reverse flow at the end of systole ($t=0.36$) and peak flow in diastole ($t=0.56$). Most of the flow quantities are computed at these time levels.

A grid independence test has been carried out for the

intention of inspecting the error connected with the grid sizes used in this investigation and is presented in Table 1. In the current situation, grid independence test has its own significance to set up the precision of the numerical results thus obtained.

Table 1 Errors connected with different grid sizes for length of separation

Grid	Time (t)	Re	Constriction Height (δ)	Separation Length at the wall
0.005 X 0.005	0.36	150	0.1	0.00
			0.2	1.08
			0.3	1.65
0.010 X 0.010	0.36	150	0.1	0.00
			0.2	1.08
			0.3	1.65
0.015 X 0.015	0.36	150	0.1	0.00
			0.2	1.05
			0.3	1.61

To verify the accuracy of the numerical scheme used in this investigation, a comparison is made with the available results of Sarifuddin *et al.* (2009) related to wall shear stress for Newtonian fluid passing through a tube having cosine shaped constriction for steady state solution (for pulsatile and sinusoidal flows) at $\mathrm{Re} = 300,\ \mathrm{St} = 1, \delta = 0$ [see Fig.2(B)]. We have also compared the axial velocity profile at $z = 2$ presented in the study of Shupti *et al.* (2015) for blood flow, modeled as a Carreau fluid, through a flexible blood vessel past a 50% cosine shaped stenosis, centered at $z = 0$,in presence of a physiological pulsatile flow at $\mathrm{Re} = 300,\ \mathrm{St} = 1$[see Fig.2(C)]. Excellent agreements are found in these comparisons which provide us immense confidence to carry on our investigation for non-Newtonian fluid model.

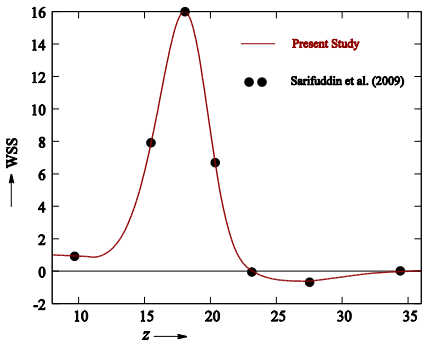

Fig. 2(B). Comparison of wall shear stress for Newtonian fluid with Sarifuddin *et al.* (2009).

With the help of the presented non-Newtonian model, a rigorous quantitative analysis has been performed for various hemodynamic parameters of major physiological significance such as wall pressure, time-averaged wall shear stress, relative residence time etc. Qualitative similarity of our findings with existing and available literature validates the applicability of our present model.

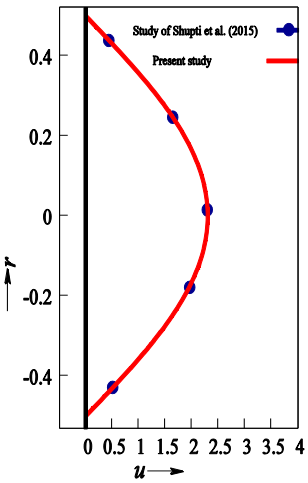

Fig. 2(C). Comparison of the axial velocity profile at z = 2 with Shupti *et al.* (2015).

At the very beginning, the wall pressure distribution at the peak flow time has been shown in Fig.3(A)–(C). A rapid fall in wall pressure is noted in the stenotic region and this sudden fall of wall pressure increases with the severity of the constriction. Because of the lower viscosity of Newtonian fluid, drop of wall pressure is less in case of Newtonian fluid than that of non-Newtonian fluid, which is in agreement with the study of Shupti *et al.* (2015). Figure 3(C) describes the effect of wall flexibility on the wall pressure distribution. It is worth noting that the flexibility of arterial wall reduces the pressure fall in the constricted region. Low pressure in the stenotic region produces a health risk as the constricted artery may collapse due to low pressure (Ku (1997), Tang *et al.* (2001)).

It is well established that the shear stress on the arterial wall plays an important role in the initiation and development of arterial diseases. Damage in the arterial wall and the blood cells may occur due to higher magnitudes of wall shear stress (Fry (1968), Sutera *et al.* (1975)). So it is of special interest to inspect the distributions of wall shear stress at the stenotic and post-stenotic regions.

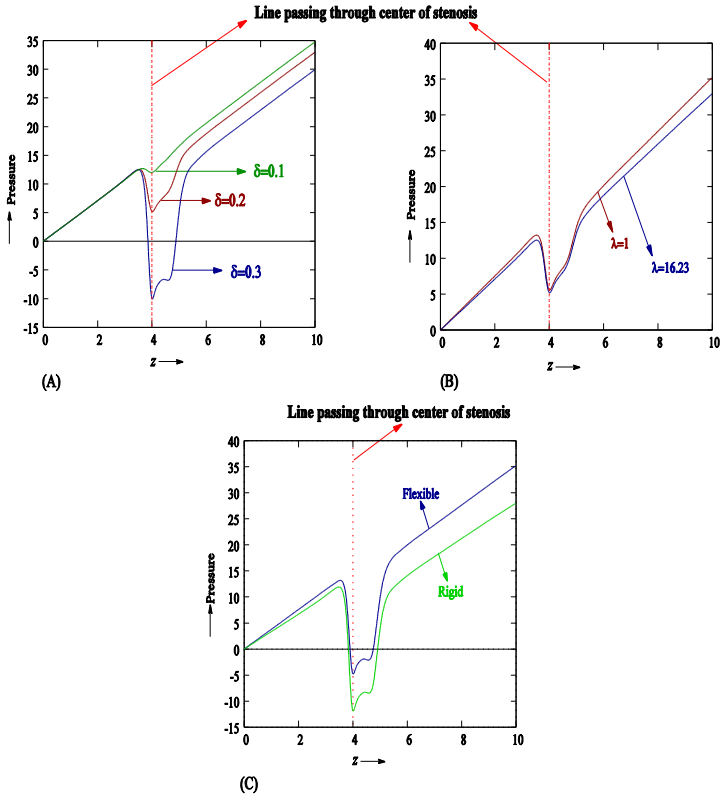

Fig. 3. Wall pressure distribution at t=0.14 for (A) different δ and $\lambda = 16.23, \Lambda = 3.313, n = 0.3568, Sc = 3,\ \mathrm{Re} = 150,\ \mathrm{St} = 0.1$; (B) different λ and $\delta = 0.2, \Lambda = 3.313, n = 0.3568,\ Sc = 3, \mathrm{Re} = 150, \mathrm{St} = 0.1$; (C) rigid and flexible tube and $\delta = 0.2, \lambda = 16.23, \Lambda = 3.313, n = 0.3568,\ Sc = 3, \mathrm{Re} = 150,\ \mathrm{St} = 0.1$.

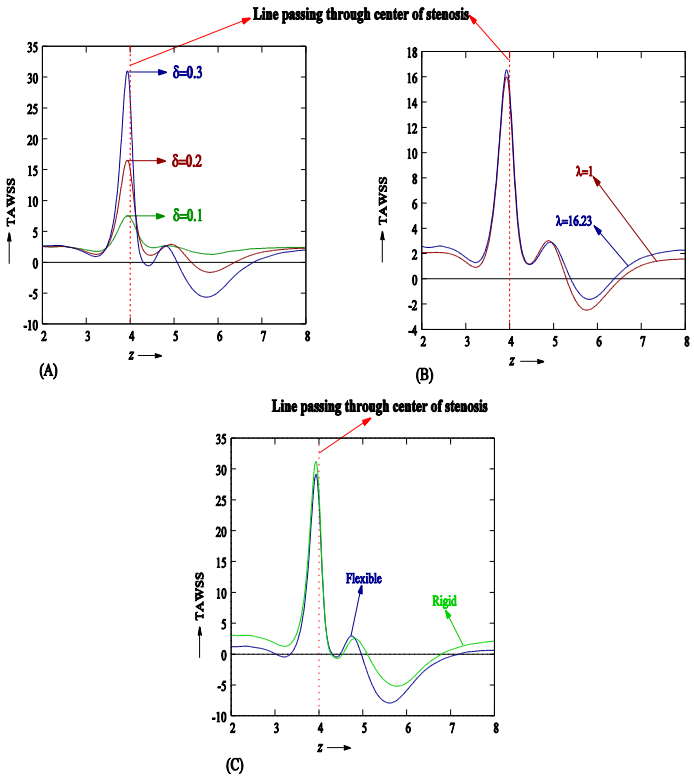

Fig. 4. Time-averaged wall shear stress distribution for (A) different $\delta$and $\lambda = 16.23, \Lambda = 3.313, n = 0.3568, Sc = 3, \mathrm{Re} = 150, \mathrm{St} = 0.1$; (B) different$\lambda$ and $\delta = 0.2, \Lambda = 3.313, n = 0.3568, Sc = 3, \mathrm{Re} = 150, \mathrm{St} = 0.1$; (C) rigid and flexible tube and $\delta = 0.2, \lambda = 16.23, \Lambda = 3.313, n = 0.3568,\ Sc = 3, \mathrm{Re} = 150,\ \mathrm{St} = 0.1$.

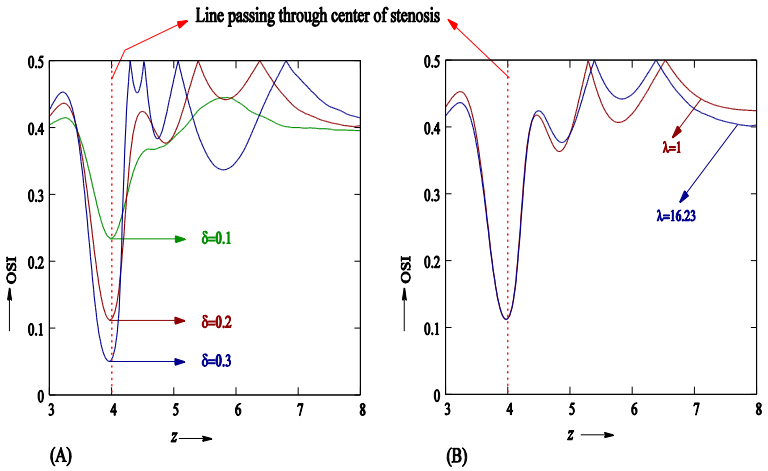

Fig. 5. Oscillatory shear index for (A) different δand $\lambda = 16.23, \Lambda = 3.313, n = 0.3568, Sc = 3, Re = 150, St = 0.1$; (B) different λ and $\delta = 0.2, \Lambda = 3.313, n = 0.3568, Sc = 3, Re = 150, St$ =0.1.

The time-averaged wall shear stress may be defined as

$$TAWSS = \int_0^1 \tau_w \, dt \tag{37}$$

Distributions of time-averaged wall shear stress for variations of δ and λ are presented in Fig.4(A) and Fig.4(B). One may note that the time-averaged wall shear stress increases significantly in the constricted part and attains its maximum (in the global sense) slightly upstream of the stenosis throat. Significantly, a second peak is also observed in the downstream side. In the rear side of the constriction, wall shear stress becomes negative in some region. This negative value of wall shear stress indicates the flow separation region. Flow separation modifies the flow structure, forms vortex and the length of this region gives an idea about the size of vortex. Formation of these recirculation regions is of pathological significance, since these regions may prolong the residing time of blood constituents which may eventually pass onto the arterial wall and form secondary stenosis. One may observe that the peak value of the $TAWSS$ and the time-averaged length of flow separation increases with severity of stenosis. For $\delta = 0.3$ (51% area reduction), two separation regions are observed: a smaller separation zone slightly downstream of the throat and a larger separation zone distal from the throat. The length of separation region for the later one increases with the stenosis height [Fig.4(A)]. Peak value of $TAWSS$ rises up, but the time-averaged length of flow separation reduces in case of non-Newtonian model compared to Newtonian model, which are consistent with the findings of Molla *et al.* (2011) [Fig.4(B)].

A comparison between the distributions of $TAWSS$ for rigid and flexible tubes are made through Fig.4(C). $TAWSS$ distribution shows a greater peak value slightly upstream of the throat in case of rigid wall than that of flexible wall. However, the recirculation zone in the downstream side of the constriction is smaller in a rigid tube compared to that in a flexible tube. Advancement of atherosclerosis reduces the wall distensibility, which, in turn, may increase the risk of rupture of the plaque by elevating the peak shear stress.

Another significant hemodynamic wall parameter is the oscillatory shear index which is defined as (Buchanan *et al.* 1999).

$$OSI = 0.5\left(1 - \left|\int_0^1 \tau_w \, dt\right| / \int_0^1 |\tau_w| \, dt\right) \tag{38}$$

and indicates the cyclic departure of the wall shear stress from its predominant axial direction. The OSI varies between 0 (for no-cyclic variation of WSS vector) and 0.5 (for 180^0 deflection of WSS vector) and the peak values indicate the locations of the time-averaged separation and reattachment points.

Figure 5 exhibits the distribution of OSI for different δ and λ. It is found that the distribution of OSI becomes more uneven and oscillatory in the post-stenotic region. The OSI has two or four characteristic peaks ($OSI|_{max} = 0.5$) at the time-averaged separation and reattachment points respectively for $\delta = 0.2$ or $\delta = 0.3$. In case of $\delta = 0.1$, no such points exist. It is observed that the first peak, representing the separation point and the second peak, representing the reattachment point of the vortex, formed in the region $5 \leq z \leq 7$, move in the upstream and downstream direction respectively with severity of the stenosis or with decreasing viscosity and extend the time-averaged length of the flow separation region. As the imposed flow profile is not always forward, $OSI|_{min}$>0.

Normally, the mass flux from the blood stream onto the arterial wall is measured with the help of the Sherwood number. For a better insight into the mass transfer phenomenon in a pulsatile flow through a constricted artery, the distributions of the time-averaged Sherwood number

$$TASh = \int_0^1 Sh \, dt \tag{39}$$

over the entire stenosed arterial segment are computed for variations of δ, λ and Sc and are depicted in Fig.6(A)–(C). One may observe from these figures that the maximum (in the global sense)

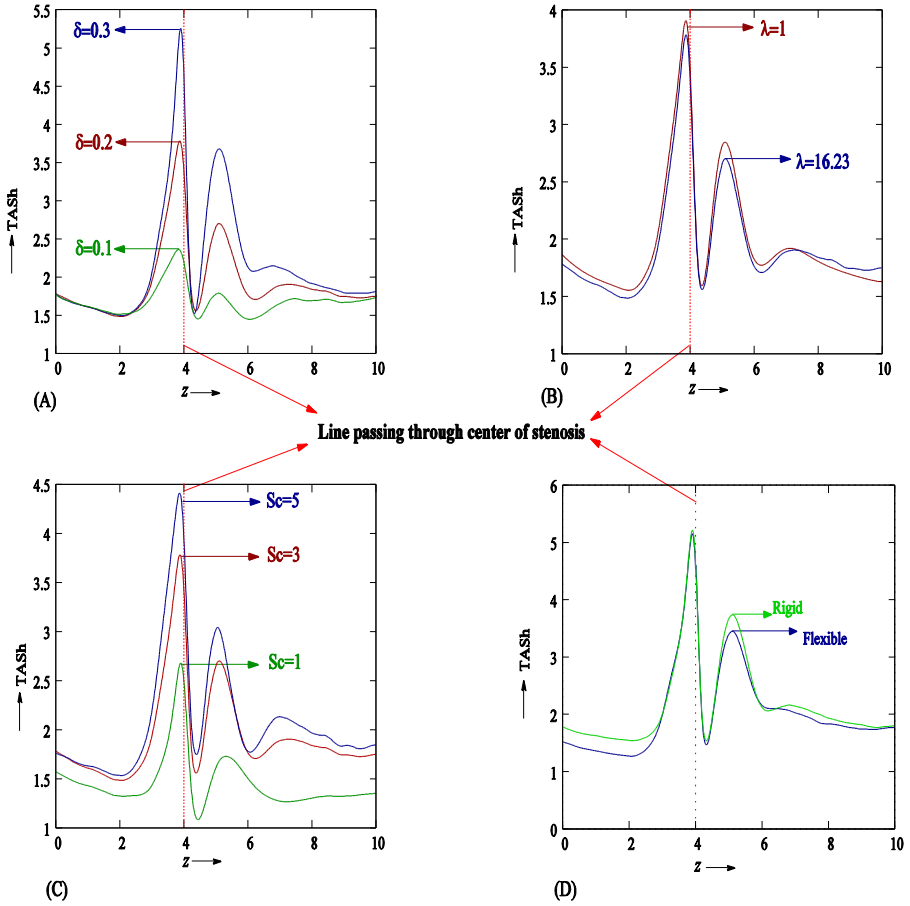

Fig. 6: Distribution of Time-averaged Sherwood number for (A) different δ and $\lambda = 16.23, \Lambda = 3.313, n = 0.3568, Sc = 3, \mathrm{Re} = 150, \mathrm{St} = 0.1$; (B) different λ and $\delta = 0.2$, $\Lambda = 3.313, n = 0.3568, Sc = 3$, $\mathrm{Re} = 150$, $\mathrm{St} = 0.1$; (C) different Sc and $\lambda = 16.23$, $\Lambda = 3.313, n = 0.3568, \delta = 0.2, \mathrm{Re} = 150, \mathrm{St} = 0.1$; (D) rigid and flexible tube and $\delta = 0.2, \lambda = 16.23, \Lambda = 3.313, n = 0.3568$, $Sc = 3, \mathrm{Re} = 150$, $\mathrm{St} = 0.1$.

mass transfer rate occurs slightly upstream of the stenosis throat in all cases like the case of the time-averaged wall shear stress. This result agrees qualitatively well with that of Kaazempur-Mofrad *et al.* (2005) and Sarifuddin *et al.* (2009). In the rear side of the stenosis, distribution of $TASh$ becomes oscillatory and twoprominent peaks are noted. This phenomenon could explain the formation of multiple stenoses observed in clinical practice (DeBakey *et al.* 1985) with the enlargement of existing one. Mass transfer rate over the entire region increases with the severity of the constriction or with increasing Schmidt number. Mass transfer rate reduces in case of non-Newtonian fluid compared to Newtonian fluid. Thus non-Newtonian fluid behaviour helps to slow down the advancement of atherosclerosis.

Figure 6(D) represents the fact that the mass transfer rate from the blood stream into the arterial wall is more in case of a rigid tube compared to a flexible tube. Thus once a mild stenosis is formed, it further helps to propagate the disease by decreasing the distensibility of vessel wall and the situation deteriorates in course of time.

Effect of the pulsatile nature of blood flow on the concentration profile is reflected through the Figs.7(A)-(C). At the systolic peak flow time, we see that the mass concentration of the solute is getting dispersed more in the downstream side of the constriction than in the upstream side. A vortex is about to form just in the lee of the stenosis. At $t = 0.36$ i.e. at the maximum back flow time dispersion of concentration takes place both in the fore and aft side of the stenosis. Mass transfer is greater in the fore side and the previously formed vortex has become larger and moved in the rear side of the constriction. A weak vortex in the upstream side is seen. At the diastolic peak flow time mass transfer has again taken place more in the rear side of the stenosis. The upstream vortex has almost disappeared and the downstream vortex has become larger and weaker and moved further downstream. With the advancement of time this vortex moves downstream and finally disappears.

Figures 8(A)-(C) depict the flow structure for various degrees of constriction at $t = 0.36$. With increasing severity of the stenosis, strength of the downstream vortex increases and another weak vortex is noted to be formed just after the throat. As the flow moves towards the throat of the stenosis, the streamlines traces the sketch of the constricted wall with a

secondary flow which helps in creating two flow separation zones in the diverging section of the constriction and ultimately the streamlines recover its normal structure later on i.e. distal to the constricted region.

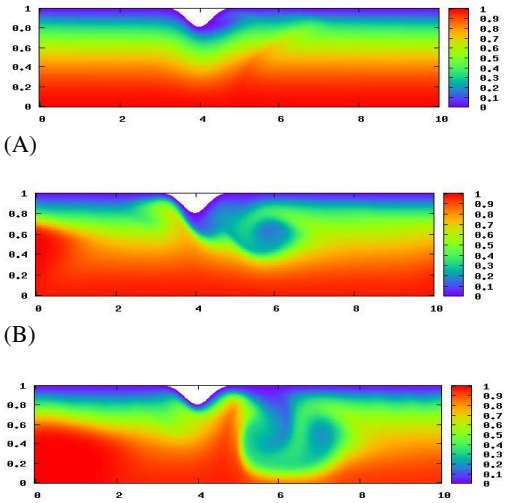

(A)

(B)

(C)

Fig. 7. Concentration profile for $\delta = 0.2, \lambda = 16.23, \Lambda = 3.313, n = 0.3568, Sc = 3, \mathrm{Re} = 150, \mathrm{St} = 0.1$ at (A) $t = 0.14$; (B) $t = 0.36$; (C) $t = 0.56$.

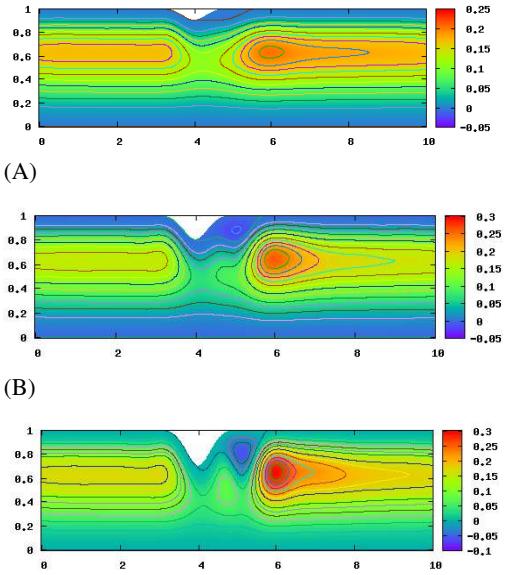

(A)

(B)

(C)

Fig. 8.Streamlines for (A) $\delta = 0.1$; (B) $\delta = 0.2$; (C) $\delta = 0.3$ at $t = 0.36$ and $\lambda = 16.23, \Lambda = 3.313, n = 0.3568, Sc = 3, \mathrm{Re} = 150, \mathrm{St} = 0.1$.

Figures 9(A)-(C) reveal the consequence of severity of constriction on the distribution of mass concentration at $t = 0.36$. As it is expected, concentration profiles for various degrees of constriction closely mirror the flow structures.

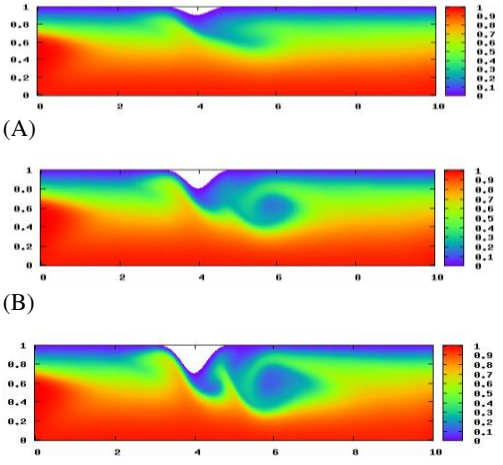

(A)

(B)

(C)

Fig. 9. Concentration profile for (A) $\delta = 0.1$; $\delta = 0.2$; (C) $\delta = 0.3$ at $t = 0.36$ and $\lambda = 16.23, \Lambda = 3.313, n = 0.3568, Sc = 3, \mathrm{Re} = 150, \mathrm{St} = 0.1$.

10. CONCLUSIONS

Localized narrowing of an artery disturbs normal blood flow and fluid dynamic factors play a significant role in the development of the disease. It is well established that mathematical models and numerical simulations offer an efficient non-invasive technique to examine probable grounds and effects of such disease. A flexible arterial model based on the mass transfer to the flowing blood past a bell shaped stenosis in its lumen is considered in the present study. A non-Newtonian shear-thinning model of blood and a physiologically realistic pulsatile flow have been considered. The main findings of this study may be summarized as follows:

i) Flow becomes more unstable in the constricted and downstream regions.

ii) Wall pressure in the stenotic region falls rapidly which may collapse the arterial wall.

iii) Wall shear stress increases dramatically in the constricted region and attains its maximum slightly upstream of the stenosis throat. Flow separation takes place in the rear side of the constriction.

iv) Maximum (in the global sense) mass transfer rate occurs slightly upstream of the stenosis throat. In the rear side of the constriction, distribution of $TASh$ becomes oscillatory. This may be a cause of the formation of multiple stenoses observed in reality.

The authors state that there is no conflict of interest.

REFERENCES

Ali, N., A. Zaman, M. Sajid, J. J. Nieto and A. Torres (2015). Unsteady non-Newtonian blood flow through a tapered overlapping stenosed catheterized vessel, *Mathematical Biosciences* 269, 94–103

Attia, R. M., M. A. A. Eldosoky and R. R. Darwish (2018). A numerical study of the blood flow behaviour in coronary artery anomalies for normal and diabetic persons. *Journal of Mechanics in Medicine and Biology* 18(2), 1850051.

Buchanan, J. R., C. Kleinstreuer, G. A. Jr, Truskey and M. Lei (1999). Relation between non-uniform hemodynamics and sites of altered permeability and lesion growth at the rabbit aorto-celiac junction. *Atherosclerosis* 143, 27-40.

Caro, C. G., J. M. Fitz-Gerald and R. C. Schroter (1971). Proposal of a shear dependent mass transfer mechanism for atherogenesis. *Clinical Science* 40(2), 5p.

Cho, Y. I. and K. R. Kensey (1991). Effects of the non-Newtonian viscosity of blood on flows in a diseased arterial vessel. Part I: Steady flows. *Biorheology* 28, 241-262.

Courant, R., K. Friedrichs and H. Lewy (1928). Über die partiellen Differenzengleichungen der mathematischen Physik. *Mathematische Annalen* 100, 32-74.

Davies, M. J. and A. C. Thomas (1985). Plaque fissuring – the cause of acute myocardial infarction, sudden ischaemic death and crescendo angina. *Brtish Heart Journal* 53(4), 363-373.

De Bakey, M. E., G. M. Lawrie and D. H. Glaeser (1985). Patterns of atherosclerosis and their surgical significance. *Annals of Surgery* 201, 115-131.

Etheir, C. R. (2002). Computational modeling of mass transfer and links to atherosclerosis. *Annals of Biomedical Engineering* 30, 461-471.

Friedman, M. H., C. B. Bargeron, D. D. Duncan, G. M. Hutchins and F. F. Mark (1992). Effects of arterial compliance and non-Newtonian rheology on correlations between intimal thickness and wall shear. *Journal of Biomechanical Engineering* 114, 317-320.

Fry, D. L. (1968). Acute vascular endothelial changes associated with increased blood velocity gradients. *Circulation Research* 22, 165-197.

Haque, M. R., M. E. Hossain and A. B. M. T. Hasan (2014). Effect of non-Newtonian behaviour on fluid structural interaction for flow through a model stenosed artery. *Procedia Engineering* 90, 358 – 363.

Kaazempur-Mofrad, M. R., S. Wada, J. G. Myers and C. R. Ethier (2005). Mass transfer and fluid flow in stenotic arteries: Axisymmetric and asymmetric models. *International Journal of Heat and Mass Transfer* 48, 4510-4517.

Ku, D. N. (1997). Blood flow in arteries, *Annual Review of Fluid Mechanics* 29, 399-434.

Ku, D. N., D. P. Giddens, C. K. Zarins and S. Glagov (1985). Pulsatile flow and atherosclerosis in the human carotid bifurcation: positive correlation between plaque location and low and oscillating shear stress. *Atherosclerosis* 5, 293-302.

Liepsch, D. (2002). An introduction tobiofluid mechanics – basic models and applications. *Journal of Biomechanics*, 415-435.

Ling, S. C. and H. B. Atabek (1972). A nonlinear analysis of pulsatile flow in arteries. *Journal of Fluid Mechanics* 55, 493-511.

Ma, P., X. Li and D.N. Ku (1994). Heat and mass transfer in a separated flow region for high Prandtl and Schmidt numbers under pulsatile conditions. *International Journal of Heat and Mass Transfer* 37, 2723-2736.

Mandal, M. S. and G. C. Layek (2014). Analysis of physiologically pulsating flow with variable blood viscosity in a doubly constricted vascular tube. *ActaTechnica* 59, 255-277.

Mandal, M. S., S. Mukhopadhyay and G. C. Layek (2012). Pulsatile flow of shear-dependent fluid in a stenosed artery. *Theoretical and Applied Mechanics* 39(3), 209-231.

Misra, J. C. and S. Chakravarty (1986). Flow in arteries in the presence of stenosis. *Journal of Biomechanics* 19, 907-918.

Misra, J. C., M. K. Patra and S. C. Misra (1993). A non-Newtonian fluid model for blood flow through arteries under stenotic conditions. *Journal of Biomechanics* 26, 1129-1141.

Molla, M. M. and M. C. Paul (2012). LES of non-Newtonian physiological blood flow in a model of arterial stenosis, *Medical Engineering & Physics* 34, 1079–1087.

Mukhopadhyay, S., M. S. Mandal and S. Mukhopadhyay (2018a). Numerical simulation of physiologically relevant pulsatile flow of blood with shear-rate-dependent viscosityin a stenosed blood vessel. *International Journal of Biomathematics* 11(06), 1-22.

Mukhopadhyay, S., M. S. Mandal and S. Mukhopadhyay (2019). Effects of variable viscosity on pulsatile flow of blood in a tapered stenotic flexible artery. *Mathematical Methods in Applied Sciences* 42(2), 488-504.

Mukhopadhyay, S., M. S. Mandal and S. Mukhopadhyay, (2018b). Dynamic response of pulsatile flow of blood in a stenosed tapered artery. *Mathematical Methodsin Applied Sciences* 41(10), 3885-3899.

Mukhopadhyay, S., P. R. De, M. S. Mandal and G. C. Layek (2011). Analysis of flow fields in a flexible tube with periodic constriction. *Applications and Applied Mathematics* 6, 304-322.

Nakamura, M. and T. Sawada (1990). Numerical study on the unsteady flow of non-Newtonian fluid. *Journal of Biomechanical Engineering* 112, 100-103.

Nandakumar, N., K. C. Sahu and M. Anand (2015). Pulsatile flow of a shear-thinning model for blood through a two dimensional stenosed channel. *European Journal of Mechanics - B/Fluids* 49, 29-35.

Nejad, A. A., Z. Talebi, D. Cheraghali, A. S. Zahiri and M. Norouzi (2018). Pulsatile flow of non-Newtonian blood fluid inside stenosed arteries: investigating the effects of viscoelastic and elastic walls, arteriosclerosis and polycythemiadiseases, *Computer Methods and Programs in Biomedicine* 154, 109–122.

Nerem, R. E. (1992). Vascular fluid mechanics, the arterial wall and arteriosclerosis. *Journal of Biomechanical Engineering* 114, 274-282.

Phillips, W. M. and S. Deutsch (1975). Toward a constitutive equation for blood. *Biorheology* 12, 383-389.

Pontrelli, G. (2001). Blood flow through an axisymmetric stenosis. Proceedings of the Institutionof Mechanical Engineers, Part H: *Journal of Engineering in Medicine* 215, 1-10.

Rappitsch, G., K. Perktold and E. Pernkopf (1997). Numerical modeling of shear-dependent mass transfer in large arteries", *International Journal of. Numerical. Methods in Fluids 25*, 847-857.

Razavi, A., E. Shirani and M. R. Sadeghi (2011). Numerical simulation of blood pulsatile flow in a stenosed carotid artery using different rheological models. *Journal of Biomechanics* 44, 2021-2030.

Ross, R. (1993). Atherosclerosis: a defense mechanism gone awry. *The American Journal of Pathology* 143(4), 987-1002.

Sarifuddin, Chakravarty, S., P. K. Mandal and H. I. Anderson (2009). Mass transfer to blood flowing through arterial stenosis. *ZeitschriftfürangewandteMathematik und Physik* 60, 299-323.

Shupti, S. P., M. G. Rabby and M. M. Molla (2015). Rheological behavior of physiological pulsatile flow through a model arterial stenosis with moving wall. *Journal of Fluids* 2015, 1-22.

Smedby, O. (1997). Do plaques grow upstream or downstream?. Arteriosclerosis*, Thrombosis and Vascular Biology* 17, 912-918.

Stettler, J. C., P. Niederer, M. Anliker and M. Casty (1981). Theoretical analysis of arterial hemodynamics including the influence of bifurcations, *Annals of Biomedical Engineering* 9, 165-175.

Sutera, S. P. and M. H. Mehrjardi (1975). Deformation and fragmentation of human red blood cells in turbulent flow. *Biophysical Journal* 15, 1-10.

Tang, D., C. Yang, S. Kobayashi and D. N. Ku (2001). Generalized finite difference method for 3-D viscous flow in stenotic tubes with large wall deformation and collapse. *Applied Numerical Mathematics* 38, 49-68.

Tripathi, B. and B. K. Sharma (2018). Influence of heat and mass transfer on two-phase blood flow with Joule heating and variable viscosity in the presence of variable magnetic field. *International Journal of Computational Methods*. 17(03), 1850139

Tu, C., M. Deville, L. Dheur and L. Vanderschurem (1992). Finie-element simulation of pulsatile flow through arterial stenosis. *Journal of Biomechanics* 25, 1141-1152.

Zaman, A., N. Ali, O. A. Bég and M. Sajid (2016). Heat and mass transfer to blood flowing through a tapered overlapping stenosed artery. *International Journal of Heat and Mass Transfer* 95, 1084–1095.

Zierenberg, J. R., H. Fujioka, V. Suresh, R. H. Bartlett, R. B. Hirschl and J. B. Grotberg (2006). Pulsatile flow and mass transport past a circular cylinder. *Physics of Fluids* 18,013102.